

Thermoacoustic and photoacoustic sensing of temperature

Manojit Pramanik

Lihong V. Wang

Washington University in St. Louis
Department of Biomedical Engineering
Optical Imaging Laboratory
Campus Box 1097
One Brookings Drive
St. Louis, Missouri 63130

Abstract. We present a novel temperature-sensing technique using thermoacoustic and photoacoustic measurements. This noninvasive method has been demonstrated using a tissue phantom to have high temporal resolution and temperature sensitivity. Because both photoacoustic and thermoacoustic signal amplitudes depend on the temperature of the source object, the signal amplitudes can be used to monitor the temperature. A temperature sensitivity of 0.15°C was obtained at a temporal resolution as short as 2 s, taking the average of 20 signals. The deep-tissue imaging capability of this technique can potentially lead us to *in vivo* temperature monitoring in thermal or cryogenic applications. © 2009 Society of Photo-Optical Instrumentation Engineers. [DOI: 10.1117/1.3247155]

Keywords: thermoacoustics; photoacoustics; temperature sensing; tissue phantom; tissue temperature.

Paper 09158R received Apr. 23, 2009; revised manuscript received Jul. 7, 2009; accepted for publication Aug. 6, 2009; published online Oct. 12, 2009.

1 Introduction

During thermotherapy or cryotherapy, it is necessary to monitor the temperature distribution in the tissues for the safe deposition of heat energy in the surrounding healthy tissue and efficient destruction of tumor and abnormal cells. To this end, real-time temperature monitoring with high spatial resolution (~ 1 mm) and high temperature sensitivity (1°C or better) is needed.¹ The most accurate temperature monitoring is by directly measuring the temperature with a thermocouple or thermistor. However, it is invasive, hence, generally not preferred and often not feasible. Several noninvasive temperature monitoring methods have been developed. Infrared thermography is a real-time method with 0.1°C accuracy but is limited only to superficial temperature.² Ultrasound can be applied for real-time temperature measurements with good spatial resolution and high penetration depth, but the temperature sensitivity is low.³⁻⁵ Magnetic resonance imaging has the advantages of high resolution and sensitivity, but it is expensive, bulky, and slow.^{6,7} Therefore, an accurate, noninvasive, real-time temperature measurement method needs to be developed.

The thermoacoustic (TA) and photoacoustic (PA) effects are based on the generation of pressure waves on absorption of microwave and light energy, respectively. A short microwave and laser pulse is usually used to irradiate the tissue. If thermal confinement and stress confinement conditions are met, then pressure waves are generated efficiently. The pressure rise of the generated acoustic wave is proportional to a dimensionless parameter called the Grueneisen parameter, and to the local fluence. The local fluence depends on the tissue parameters, such as the absorption coefficient, scattering co-

efficient, and anisotropy factor, and does not change significantly with temperature. However, the Grueneisen parameter, which depends on the isothermal compressibility, the thermal coefficient of volume expansion, the mass density, and the specific heat capacity at constant volume of the tissue, changes significantly with temperature. Thus, the generated TA/PA signal amplitude changes with temperature. Here, we show that by monitoring the change in the TA/PA signal amplitude, we were able to monitor the change in temperature of the object.

The TA/PA technique has been widely applied in biomedical imaging applications, such as breast cancer imaging, brain structural and functional imaging, blood-oxygenation and hemoglobin monitoring, tumor angiogenesis, and, recently, for molecular imaging.⁸⁻²² Lately, PA sensing has also been used to monitor tissue temperature.^{1,23-27} However, TA sensing of temperature has never been studied. These two techniques do not interact and can be used independently. Depending on the need, one has to choose which technique to use. The main difference between these two techniques is the contrast mechanism. For example, water and ion concentrations are the main sources of contrast in TA measurements, whereas blood and melanin are the main sources of contrast in PA measurements. Therefore, if we need to monitor the temperature of a blood vessel, then the PA technique will be more useful; whereas if we need to monitor the temperature of muscles, then the TA technique will be preferred. TA/PA temperature sensing is a noninvasive, real-time method. The TA/PA technique has the ability to image deeply (up to 5 cm) with high spatial resolution (scalable: millimeters to microns). We can monitor temperature with high temporal resolution and high temperature sensitivity (scalable with temporal resolution: ± 0.015 and $\pm 0.15^{\circ}\text{C}$ at 200 s (2000 measurements averaged) and 2 s (20 measurements averaged) resolutions,

Address all correspondence to: Lihong Wang, Washington University in St. Louis, Department of Biomedical Engineering, Optical Imaging Laboratory, Campus Box 1097, One Brookings Drive, St. Louis, MO 63130. Tel: (314) 935-6152; Fax: (314) 935-7448; E-mail: lhwang@biomed.wustl.edu

respectively). Because microwaves penetrate more deeply into tissue than light, we can potentially monitor temperature *in vivo* for locations deep inside the body.

2 Theoretical Background

If the microwave/laser excitation is much shorter than both the thermal diffusion (i.e., the excitation is in thermal confinement) and the pressure propagation (i.e., the excitation is in stress confinement) in a heated region, the fractional volume expansion dV/V can be expressed as

$$\frac{dV}{V} = -\kappa p + \beta T,$$

where κ is the isothermal compressibility, β is the thermal coefficient of volume expansion, and p and T denote changes in pressure (measured in Pascal), and temperature (in Kelvin), respectively.

When the fractional change in volume is negligible under rapid heating, the local pressure rise immediately after the microwave/laser excitation pulse can be derived as

$$p_0 = \frac{\beta T}{\kappa} = \frac{\beta}{\kappa \rho C_v} \eta_{th} A_e = \Gamma \eta_{th} A_e,$$

where ρ denotes mass density, C_v denotes specific heat capacity at constant volume, A_e is the specific optical/microwave absorption, and η_{th} is the percentage of absorbed energy that is converted to heat.

We define the Grueneisen parameter (dimensionless) as

$$\Gamma = \frac{\beta}{\kappa \rho C_v} = \frac{\beta v_s^2}{C_p} = f(T),$$

where v_s is the velocity of sound, C_p denotes the specific heat capacity at constant pressure, and T is the temperature of the object.

Therefore,

$$p_0 = f(T) \eta_{th} A_e.$$

Thus, in practice, the measured pressure signal generated due to the microwave/laser excitation can be used to monitor the temperature. Note that, here we always refer to the base temperature of the object, not the change in temperature due to the microwave/laser heating. The instantaneous temperature increase in the object due to the microwave/laser pulse heating is on the order of milliKelvin and its effect on the Grueneisen parameter is negligible. The base temperature of the object is a slowly varying parameter compared to the transient temperature increase induced by a microwave/laser pulse.

3 System Description

Figure 1(a) shows the combined TA and PA system used for sensing temperature. A similar concept of integrating light with microwaves was used earlier for a breast cancer imaging system.²¹ The plastic chamber containing the sample holder was filled with mineral oil, a nonmicrowave-absorbing material. Moreover, because mineral oil is visibly transparent, light absorption is negligible. Mineral oil also acts as a coupling medium for sound propagation, and thus, mineral oil was an

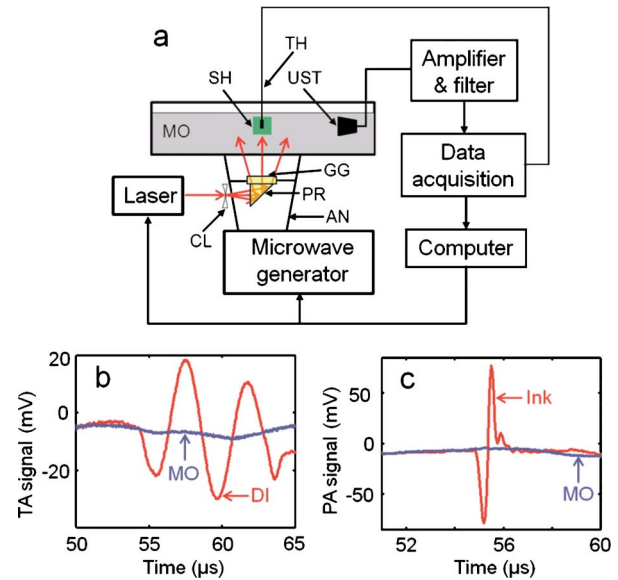


Fig. 1 (a) Schematic of the experimental setup. MO: mineral oil bath, SH: sample holder vial, UST: ultrasonic transducer, GG: ground glass, PR: prism, AN: horn antenna, CL: concave lens, TH: thermistor, (b) TA signals from a LDPE vial (i.d. 12 mm, volume 5 cc) filled with mineral oil (MO) and DI water (DI). (c) PA signals from LDPE vial filled with ink solution ($\mu_a = 30 \text{ cm}^{-1}$) and mineral oil at 532 nm wavelength.

ideal choice as a background medium for all our experiments. The microwave/laser assembly was placed under the sample holder chamber, from where it illuminated the sample by either microwave or laser, alternately, for TA/PA sensing. The microwave was delivered using a horn antenna, whereas the laser was delivered by a free-space optical assembly. The prism and ground glass of the laser illumination system were incorporated inside the microwave horn antenna. As a result, it was not necessary to mechanically switch between the microwave and laser sources: the switching was electronic and instantaneous. Light was delivered through a drilled ~ 10 -mm-diam hole in one of the narrow walls of the horn antenna. The laser beam was broadened by a concave lens placed outside the hole in the horn antenna, then reflected by the prism and homogenized by the ground glass. This type of beam expansion scheme has been used extensively before.^{13,15,28} The insertion of the optical devices inside the microwave horn antenna had no significant effect on the microwave delivery.²¹

3.1 Microwave Source

A 3.0-GHz microwave source produced pulses of 0.5- μs width, with a repetition rate of up to 100 Hz. An air-filled pyramidal horn-type antenna (WR284 horn antenna W/EEV flange, HNL Inc.) with a rectangular opening of $7.3 \times 10.7 \text{ cm}^2$ was used to deliver the microwaves to the sample. The specific absorption rate of the tissue was within the IEEE safety standards.²⁹

The horn antenna was designed to transport the transverse electric (TE) TE_{10} mode of electromagnetic (EM) waves, so the electric field was parallel (or nearly parallel for a horn) to the surface of either narrow side (y -polarized in our system) and approached zero near the inner surface of either narrow

wall. By contrast, the electric field was nonzero near the surface of either wide wall. Therefore, opening the light delivery hole on the narrower side of the horn antenna (or wave guide) minimized the power leakage.

3.2 Laser Source

The light source was a Q-switched Nd:YAG laser with a repetition rate of 10 Hz, providing 6.5-ns-wide laser pulses. The laser system could provide 400-mJ maximal output energy at 532-nm wavelength. The incident laser fluence on the sample surface was controlled to $<20 \text{ mJ/cm}^2$, conforming to the American National Standards Institute safety standards.³⁰

3.3 Detection of Ultrasound

For detecting the ultrasound signal, we used a 13-mm-diam active-area nonfocused transducer operating at 2.25 MHz central frequency (ISS 2.25 \times 0.5 COM, Krautkramer). The signal was first amplified by a low-noise pulse amplifier (5072PR, OlympusNDT), then filtered electronically, and finally recorded using a digital oscilloscope (TDS640A, Tektronix). When microwaves were the illumination source, a delay/pulse generator (SRS, DG535) triggered the microwave pulses and synchronized the oscilloscope. By contrast, during laser illumination, the sync out from the laser system synchronized the laser pulses and the data acquisition.

3.4 Temperature Sensor

A precision thermistor for laboratory applications (sealed PVC tip, resistance of 2252 Ω at 25 $^\circ\text{C}$ and accuracy of $\pm 0.1 \text{ }^\circ\text{C}$; ON-401-PP, Omega) was used to measure the temperature of the sample. The tip of the thermistor was inserted inside the sample to get an accurate measurement of the temperature. A voltage divider circuit with a dc source (Vizatek, MPS-6003L-1) converted the resistance change of the thermistor into voltage, which was recorded using the aforementioned oscilloscope. Because the current through the thermistor was very small, the self-heating was negligible.

3.5 Sample Holder Vial

Low density polyethylene (LDPE) vials with ~ 12 -mm i.d. and 5-cc volume were the sample holders for the entire study. LDPE has an acoustic impedance $Z_1=1.79$ and acoustic loss= 2.5 dB/cm at 5 MHz. The background material was mineral oil, which has an impedance $Z_2=1.19$. Intensity reflectivity (assuming normal incidence) $= (Z_2 - Z_1)^2 / (Z_2 + Z_1)^2 = 0.04$ (4%). Intensity transmittivity (assuming normal incidence) $= 4Z_2Z_1 / (Z_2 + Z_1)^2 = 0.96$ (96%). The speed of sound in LDPE $= 1.95 \text{ mm}/\mu\text{s}$; thus, the wavelength of sound in LDPE $= 0.975 \text{ mm}$ at 2 MHz. The wall thickness of the LDPE vial was $\sim 1 \text{ mm}$, which was comparable to the wavelength. Therefore, the loss of acoustic signal due to impedance mismatch was relatively small (only $\sim 4\%$). Moreover, the loss of signal due to absorption inside the LDPE was also very small, $\sim 2.5 \text{ dB/cm}$ at 5 MHz [i.e., for 1 mm thickness, the loss due to absorption would be $\sim 0.25 \text{ dB/mm}$ at 5 MHz ($\sim 2.5\%$ loss per mm of thickness)]. Moreover, our ultrasound transducer had a center frequency at 2.25 MHz. The lower the sound frequency is, the less the absorption is.

At 3 GHz, the loss tangents of water and LDPE are 0.157 and 0.00031, respectively, and the relative dielectric constants

are ~ 78 and ~ 2.26 , respectively. The amount of power (measured in watts per cubic meter) that is absorbed is given by, $P=2\pi f\epsilon_0\epsilon_r'\tan\delta E^2$, where f is the frequency (measured in Hertz), $\epsilon_0=8.854\times 10^{-12}\text{Fm}^{-1}$, ϵ_r' is the relative dielectric constant, $\tan\delta$ is the loss tangent, and E is the potential gradient (measured in volts per meter). Thus,

$$\begin{aligned} \frac{P_{\text{water}}}{P_{\text{LDPE}}} &= \left(\frac{\epsilon_{r,\text{water}}'}{\epsilon_{r,\text{LDPE}}'} \right) \left(\frac{\tan\delta_{\text{water}}}{\tan\delta_{\text{LDPE}}} \right) \\ &= \left(\frac{78}{2.26} \right) \left(\frac{0.157}{0.00031} \right) = 17479. \end{aligned}$$

Therefore, the microwave absorption of LDPE is negligible compared to that of water. Thus, there was virtually no possibility of producing TA signals from the LDPE vial because there was essentially no microwave absorption by the LDPE. Figure 1(b) shows the TA signal generated from the sample holder (LDPE vial) filled with deionized (DI) water and with mineral oil. The DI water vial produced a 48-mV peak-to-peak TA signal (red line), while no significant TA signal was generated from the vial filled with mineral oil (blue line). Therefore, the LDPE vial did not generate any detectable TA signal. We also tested the PA signal generated from the LDPE vial filled with ink solution and mineral oil, at 532 nm wavelength light. Black acrylic artists ink was diluted with water to have an absorption coefficient of $\sim 30 \text{ cm}^{-1}$ at 532 nm. A Cary 50 ultraviolet/visible spectrophotometer was used to find the absorption coefficient of the ink solution. Figure 1(c) shows the PA signals, and the ink vial produced a 156-mV peak-to-peak PA signal (red line), while with mineral oil did not produce any significant PA signal (blue line). Therefore, we concluded that the sample holder vial had no detectable effect either in TA or PA signal generation and, henceforth, all signals observed were considered to be generated from the sample placed inside the vial.

3.6 Experimental Procedure

The sample holder vial was filled with different samples, DI water for TA measurements, and ink solution for PA measurements. Two types of experiments were done. A heated sample was allowed to come to room temperature by natural convection, exchanging heat with the background medium (mineral oil). The volume of the sample was very small compared to the mineral oil; thus, the temperature rise of the mineral oil was neglected. The TA/PA signal was recorded with time as the sample temperature decreased to room temperature. The thermistor was inserted inside the sample to monitor the actual temperature. Next, cold sample was allowed to reach room temperature by natural convection, exchanging heat with mineral oil, and the TA/PA signal was recorded with time as the sample temperature increased to room temperature. The actual temperature of the sample was also monitored using a thermistor as before. Note that, for the decreasing and increasing temperature experiments, the sample holder position may have altered slightly. The sample holder was removed, refilled with cold/hot sample, and then placed back in the system.

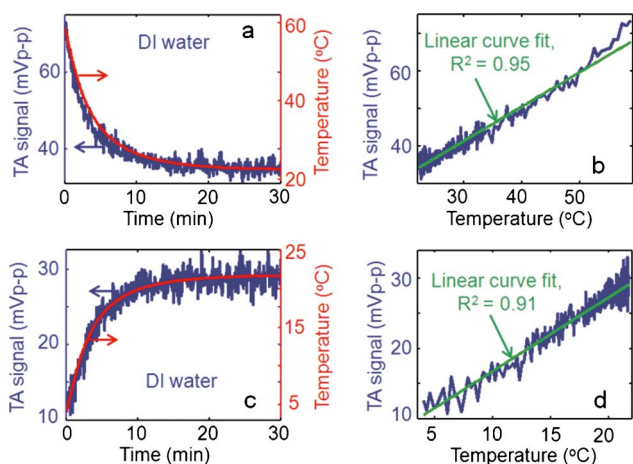


Fig. 2 (a) TA signal and actual temperature of DI water as heated DI water was allowed to come to room temperature, (b) TA signal versus temperature, which shows almost a linear relationship. Green line is the linear curve fitting with an R^2 of 0.95. (c) TA signal and the actual temperature of DI water as cold DI water was allowed to come to room temperature, (d) TA signal versus temperature, which shows almost a linear relationship. Green line is the linear curve fitting with an R^2 of 0.91. (Color online only.)

4 Results and Discussions

Figure 2(a) shows the peak-to-peak TA signal amplitude and the actual temperature of the DI water. The TA signal decreased as the DI water cooled to room temperature with time. The TA signal follows the actual temperature profile (red line) very well. Figure 2(b) plots the TA signal versus the temperature of the sample. The green line shows a linear curve fit with an R^2 of 0.95. A linear relationship between the actual temperature and the TA signal was observed. Figure 2(c) shows the TA signal increased when the cold DI water temperature reached room temperature. The TA signal follows the actual temperature profile (red line) very well. Figure 2(d) plots the TA signal versus the temperature of DI water, and the green line shows a linear curve fit with an R^2 of 0.91. A linear relationship between the temperature and the TA signal was observed. For water in this temperature range, the Grueneisen parameter is a linear function of temperature^{31,32} and, therefore, the TA signal amplitude also varies linearly with the temperature.

Similar experiments were done for PA measurements with ink solution as a sample. Figure 3(a) shows the PA signal generated from the ink solution and the actual temperature. Once again, the PA signal decreased as the solution temperature approached room temperature, and followed the actual temperature profile (red line) very well. Figure 3(b) plots the PA signal versus temperature, with the green line showing a linear curve fit with an R^2 of 0.98. Next, a cold ink solution was allowed to reach room temperature. The PA signal increased as the temperature of the solution increased [Fig. 3(c)] and followed the actual temperature profile (red line) very well. Figure 3(d) plots the PA signal versus the temperature with the green line showing a linear curve fit with an R^2 of 0.98.

Table 1 summarizes the TA/PA measurements. The number of measurements averaged was 20 for each data point, and as

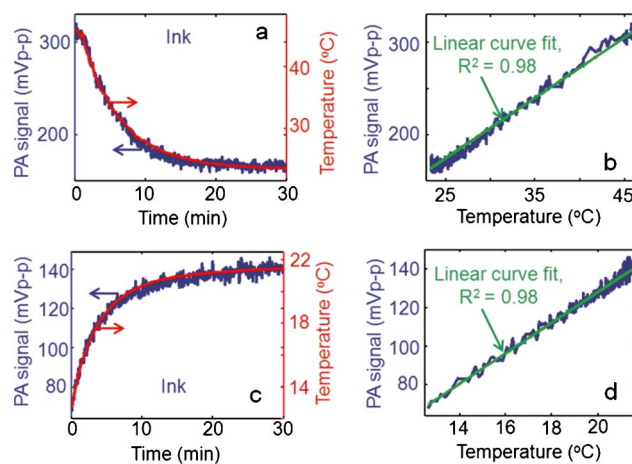


Fig. 3 (a) PA signal and actual temperature of diluted black ink solution ($\mu_a=30 \text{ cm}^{-1}$) as the heated sample was allowed to come to room temperature, (b) PA signal versus temperature, which shows almost a linear relationship. Green line is the linear curve fitting with an R^2 of 0.98. (c) PA signal and the actual temperature of ink solution as cold solution was allowed to come to room temperature, (d) PA signal versus temperature, which shows almost a linear relationship. Green line is the linear curve fitting with an R^2 of 0.98. (Color online only.)

the microwave/laser was operating at 10 Hz pulse repetition rate, the temporal resolution was 2 s. We can see the change in signal per degree change in temperature is slightly higher for increasing temperature than for decreasing temperature. It was 3.6% for increasing temperature (compared to 3.0% for decreasing temperature) in the case of TA measurements, and 5.9% for increasing temperature (compared to 4.1% for decreasing temperature) in the case of PA measurements.

Figure 4(a) shows how the Grueneisen parameter of water varies with temperature ($\Gamma = \beta v_s^2 / c_p$) in the temperature range of interest.^{31,32} It increases linearly with temperature, with a higher slope within the range 0–20°C than within the range 20–100°C (the slope in the range 0–20°C is 1.48 times the slope in the range 20–100°C). This agrees with our observation in both TA and PA measurements for increasing and decreasing temperature. For the TA measurements, the slope in the range 4–22°C was 1.16 times the slope in the range 23–58°C, and for the PA measurements the slope in the range 13–22°C was 1.44 times the slope in the range 24–46°C. We can also see a slight difference in the signals, depending on the direction from which the sample comes to equilibrium. In the case of TA measurements, the equilibrium signals were 35.1 and 28.9 mV (17.6% difference) for equilibrium reached from cooling and warming, respectively. The corresponding equilibrium temperatures were 22.59 and 21.66°C. There was an almost 1°C difference between the two equilibrium temperatures. After accounting for this difference, we see a ~14% [$17.6\% - (3.0\% + 3.6\%)/2 = 14.3\%$] signal discrepancy. In the case of PA measurements, the equilibrium signals were 166.7 and 140.3 mV (15.8% difference) and the equilibrium temperatures were 23.57 and 21.41°C, respectively. There was an almost 2°C temperature difference between the two equilibrium temperatures. After accounting for this difference, we see a ~6% [$15.8\% - 2 \times (4.1\%$

Table 1 TA/PA signal change per degree centigrade change in temperature of DI water/ink solution in a tube.

		T_{\max} (°C)	T_{\min} (°C)	S_{\max} (mV)	S_{\min} (mV)	Signal change	
						(%/°C)	(mV/°C)
TA measurements	Decreasing temperature	58.7	22.6	73.3	35.1	3.0	1.0
	Increasing temperature	21.7	4.0	28.9	10.7	3.6	1.0
PA measurements	Decreasing temperature	46.0	23.6	319.8	166.7	4.1	6.8
	Increasing temperature	21.4	12.6	140.3	67.6	5.9	8.3

+5.9%)/2=5.8%] signal discrepancy. The TA/PA signal generated from the sample is dependent on various factors, such as the orientation of the sample holder and the spatial distribution of microwaves/light on the sample surface. Therefore, the absolute signal is very sensitive to the position of the sample holder. Because the sample holder position was altered slightly between experiments, these variations in signal could arise. If the sample holder had been fixed in its position between different experiments (increasing and decreasing temperatures), the variation in the signal amplitudes would have been less. Of course, when the technology is used to monitor thermal therapy, the sample will be held stationary.

The temperature measurement precision was $\pm 1^\circ\text{C}$ for TA measurements and $\pm 0.5^\circ\text{C}$ for PA measurements. Here, we have used the terms precision and sensitivity synonymously. The temperature precision is calculated based on the

uncertainty in the mean value of the measurements (standard error). The precision would improve if we took a larger sample size. Figure 4(b) shows how the temperature precision typically varies with the number of measurements averaged for TA measurements. As expected, the standard error decreased as a factor of the square root of the number of measurements averaged. The greater the number of measurements averaged is, the less the standard error is, and hence, the higher the precision. The plot is on a log-log scale, yielding a linear curve with -0.47 slope (mean slope = -0.40 ± 0.05 , for seven repeated experiments). In an ideal situation, the slope should be -0.5 . It is observed that the temperature precision could be as high as $\pm 0.1^\circ\text{C}$ with >2000 measurements averaged. Of course, the increased precision comes at the expense of temporal resolution. With the current microwave source (a maximum 100-Hz pulse repetition rate), the temporal resolution could be as long as 20 s to achieve a temperature precision of $\pm 0.1^\circ\text{C}$. However, employing a higher repetition rate microwave source can eventually give us even higher temperature precision with practical temporal resolution. Similarly, Figure 4(c) shows how the temperature precision varied with the number of measurements averaged for PA measurements. As expected, the precision could be as high as $\pm 0.1^\circ\text{C}$ with >1000 measurements averaged. As before, the plot is on a log-log scale, with a linear curve with -0.44 slope (mean slope = -0.40 ± 0.03 , for five repeated experiments). Note that the precision varies from sample to sample depending on the signal-to-noise (SNR). We will show later that, for saline and turkey breast tissue, we obtained even higher precision in temperature based on TA measurements with 20 measurements averaged.

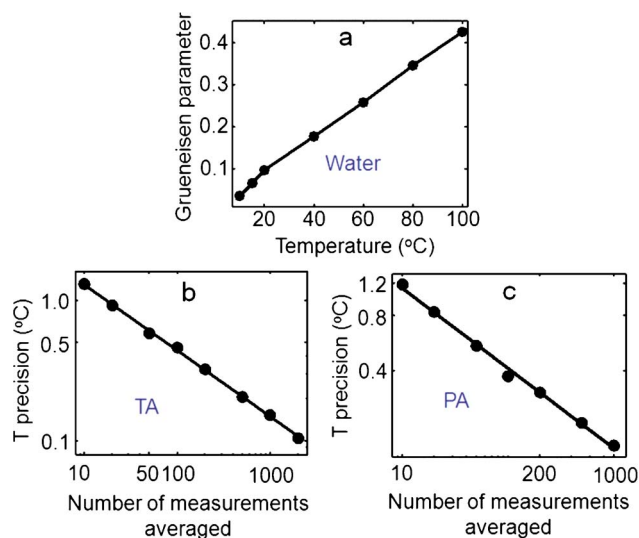


Fig. 4 (a) Variation of the Grueneisen parameter of water with temperature.^{31,32} (b) Temperature precision versus number of measurements averaged for TA measurements in log-log scale. The plot shows a linear curve with a slope of -0.47 . (c) Temperature precision versus number of measurements averaged for PA measurements in log-log scale. The plot shows a linear curve with a slope of -0.44 .

4.1 Saline/Tissue Temperature Monitoring Using TA Measurements

We also used saline (0.9% w/v of NaCl in water) and turkey breast tissue as a phantom. The same experimental procedures were followed as before. Figure 5(a) shows that the TA signal decreased as the temperature of the saline decreased. The TA signal followed the actual temperature profile (red line) very closely. Figure 5(b) shows a second-order curve fit (green line) for the TA signal versus the temperature of saline with an

Table 2 Saline and turkey breast tissue temperature monitoring using TA measurements. The precision is based on averaging 20 measurements.

	T_{\max} (°C)	T_{\min} (°C)	S_{\max} (mV)	S_{\min} (mV)	Signal change		Precision (°C)
					(%/°C)	(mV/°C)	
Saline	49.0	21.9	196.6	75.3	5.9	4.5	±0.3
Turkey breast tissue	37.0	23.6	335.6	184.5	6.1	11.3	±0.15

R^2 of 0.99. Figure 5(c) shows that the TA signal decreased as the temperature of the tissue decreased. The TA signal followed the actual temperature profile (red line) very closely. Figure 5(d) shows a second-order curve fit (green line) for the TA signal versus the temperature with an R^2 of 0.99. Table 2 summarizes the TA measurements for the sensing of the saline and turkey breast tissue temperatures. As before, 20 measurements were averaged. For the saline, there was ~5.9% change in TA signal, whereas for tissue there was ~6.1% change in signal per degree centigrade change in temperature. The TA signal generated from the tissue had a very high SNR of ~100 at room temperature (~24°C). Thus, the minimum detectable signal change (i.e., noise-equivalent signal change) is ~1%, which gives us a temperature sensitivity of ~0.15°C (=1/6.1). However, if the SNR is improved, the sensitivity could be even better. The temperature precision was ±0.15°C (with 20 measurements averaged) based on the standard error. As discussed before, taking the average of a greater number of signals (>2000) the precision could be improved to ±0.015°C.

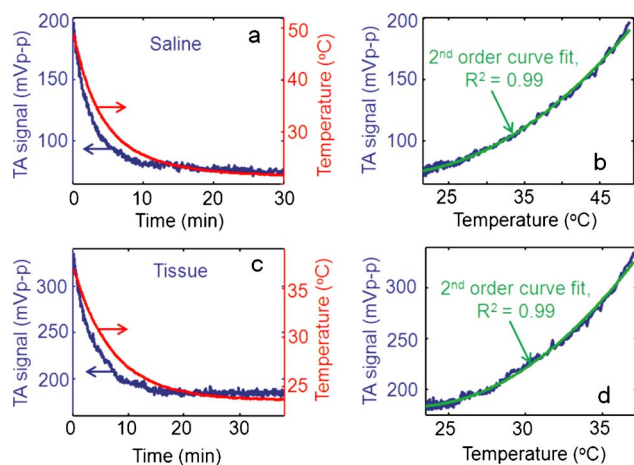


Fig. 5 (a) Temperature monitoring of saline using TA measurements. TA signal followed the actual temperature profile. (b) TA signal versus temperature. A second-order relationship (green line) was observed with an R^2 of 0.99. (c) Temperature monitoring of turkey breast tissue using TA measurements. TA signal and actual temperature of turkey breast tissue as heated tissue was allowed to come to room temperature. (d) TA signal versus temperature. A second-order relationship was observed. The green curve shows a second-order curve fit with an R^2 of 0.99. (Color online only.)

5 Conclusions

A novel temperature-sensing method based on TA and PA measurements is reported. This noninvasive method has deep-tissue-sensing capabilities. Depending on the tissue types, either the TA or PA component, or both, could be used. We monitored temperature of DI water thermoacoustically within 5–60°C, and photoacoustically monitored the temperature of diluted ink solution within 12–46°C. We also showed that the TA-based measurements could be used for saline and turkey breast tissue temperature monitoring. The temperature sensitivity was 0.15°C with 2 s (20 measurements averaged) temporal resolution. Measurement precision could be improved by taking more signal averages. In the future, we would like to continue the monitoring of temperature *in vivo* using both TA and PA sensing for various applications, such as temperature monitoring for tissue during radiofrequency ablation, radiation therapy, photothermal therapy, photodynamic therapy, cancer treatment using high intensity focuses ultrasound (HIFU), and drug delivery using HIFU.

Acknowledgments

This work was sponsored by National Institutes of Health Grants No. R01 EB000712, No. R01 NS46214 (Bioengineering Research Partnerships), No. R01 EB008085, and No. U54 CA136398 (Network for Translational Research). L.W. has a financial interest in Endra, Inc., which, however, did not support this work. We thank Claire Cobley for her help with the spectrophotometer and James Ballard for helping us with the manuscript preparation.

References

1. I. V. Larina, K. V. Larin, and R. O. Esenaliev, "Real-time optoacoustic monitoring of temperature in tissues," *J. Phys. D* **38**(15), 2633–2639 (2005).
2. A. J. Welch and M. J. C. Van Gemert, *Optical-Thermal Response of Laser-Irradiated Tissue*, Plenum, New York (1995).
3. R. Seip and E. S. Ebbini, "Noninvasive estimation of tissue temperature response to heating fields using diagnostic ultrasound," *IEEE Trans. Biomed. Eng.* **42**(8), 828–839 (1995).
4. R. MaassMoreno and C. A. Damianou, "Noninvasive temperature estimation in tissue via ultrasound echo-shifts, I. analytical model," *J. Acoust. Soc. Am.* **100**(4), 2514–2521 (1996).
5. R. Seip, P. VanBaren, C. A. Cain, and E. S. Ebbini, "Noninvasive real-time multipoint temperature control for ultrasound phased array treatments," *IEEE Trans. Ultrason. Ferroelectr. Freq. Control* **43**(6), 1063–1073 (1996).
6. S. J. Graham, M. J. Bronskill, and R. M. Henkelman, "Time and temperature dependence of MR parameters during thermal coagulation of ex vivo rabbit muscle," *Magn. Reson. Med.* **39**(2), 198–203 (1998).

7. P. Steiner, R. Botnar, B. Dubno, G. G. Zimmermann, G. S. Gazelle, and J. F. Debatin, "Radio-frequency-induced thermoablation: monitoring with T1-weighted and proton-frequency-shift MR imaging in an interventional 0.5-T environment," *Radiology* **206**(3), 803–810 (1998).
8. C. G. A. Hoelen, F. F. M. de Mul, R. Pongers, and A. Dekker, "Three-dimensional photoacoustic imaging of blood vessels in tissue," *Opt. Lett.* **23**(8), 648–650 (1998).
9. R. A. Kruger, K. K. Kopecky, A. M. Aisen, D. R. Reinecke, G. A. Kruger, and W. L. Kiser, "Thermoacoustic CT with radio waves: a medical imaging paradigm," *Radiology* **211**(1), 275–278 (1999).
10. L. H. V. Wang, X. M. Zhao, H. T. Sun, and G. Ku, "Microwave-induced acoustic imaging of biological tissues," *Rev. Sci. Instrum.* **70**(9), 3744–3748 (1999).
11. R. A. Kruger, K. D. Miller, H. E. Reynolds, W. L. Kiser, D. R. Reinecke, and G. A. Kruger, "Breast cancer *in vivo*: contrast enhancement with thermoacoustic CT at 434 MHz—feasibility study," *Radiology* **216**(1), 279–283 (2000).
12. A. A. Oraevsky, E. V. Savateeva, S. V. Solomatin, A. A. Karabutov, V. G. Andreev, Z. Gatalica, T. Khamapirad, and P. M. Henrichs, "Optoacoustic imaging of blood for visualization and diagnostics of breast cancer," *Proc. SPIE* **4618**, 81–94 (2002).
13. X. D. Wang, Y. J. Pang, G. Ku, X. Y. Xie, G. Stoica, and L. H. V. Wang, "Noninvasive laser-induced photoacoustic tomography for structural and functional *in vivo* imaging of the brain," *Nat. Biotechnol.* **21**(7), 803–806 (2003).
14. Y. W. Wang, X. Y. Xie, X. D. Wang, G. Ku, K. L. Gill, D. P. O'Neal, G. Stoica, and L. H. V. Wang, "Photoacoustic tomography of a nanoshell contrast agent in the *in vivo* rat brain," *Nano Lett.* **4**(9), 1689–1692 (2004).
15. G. Ku, B. D. Fornage, X. Jin, M. H. Xu, K. K. Hunt, and L. H. V. Wang, "Thermoacoustic and photoacoustic tomography of thick biological tissues toward breast imaging," *Technol. Cancer Res. Treat.* **4**(5), 559–565 (2005).
16. G. Ku, X. D. Wang, X. Y. Xie, G. Stoica, and L. H. V. Wang, "Imaging of tumor angiogenesis in rat brains *in vivo* by photoacoustic tomography," *Appl. Opt.* **44**(5), 770–775 (2005).
17. H. F. Zhang, K. Maslov, G. Stoica, and L. H. V. Wang, "Functional photoacoustic microscopy for high-resolution and noninvasive *in vivo* imaging," *Nat. Biotechnol.* **24**(7), 848–851 (2006).
18. J. Gamelin, A. Aguirre, A. Maurudis, F. Huang, D. Castillo, L. V. Wang, and Q. Zhu, "Curved array photoacoustic tomographic system for small animal imaging," *J. Biomed. Opt.* **13**(2), 024007 (2008).
19. M. L. Li, J. T. Oh, X. Y. Xie, G. Ku, W. Wang, C. Li, G. Lungu, G. Stoica, and L. H. V. Wang, "Simultaneous molecular and hypoxia imaging of brain tumors *in vivo* using spectroscopic photoacoustic tomography," in *Proc. IEEE* Vol. **96**, pp. 481–489 (2008).
20. K. H. Song, E. W. Stein, J. A. Margenthaler, and L. V. Wang, "Non-invasive photoacoustic identification of sentinel lymph nodes containing methylene blue *in vivo* in a rat model," *J. Biomed. Opt.* **13**(5), 054033 (2008).
21. M. Pramanik, G. Ku, C. H. Li, and L. H. V. Wang, "Design and evaluation of a novel breast cancer detection system combining both thermoacoustic (TA) and photoacoustic (PA) tomography," *Med. Phys.* **35**(6), 2218–2223 (2008).
22. A. De La Zerda, C. Zavaleta, S. Keren, S. Vaithilingam, S. Bodapati, Z. Liu, J. Levi, B. R. Smith, T. J. Ma, O. Oralkan, Z. Cheng, X. Y. Chen, H. J. Dai, B. T. Khuri-Yakub, and S. S. Gambhir, "Carbon nanotubes as photoacoustic molecular imaging agents in living mice," *Nat. Nanotechnol.* **3**(9), 557–562 (2008).
23. S. Y. Emelianov, S. R. Aglyamov, A. B. Karpiouk, S. Mallidi, S. Park, S. Sethuraman, J. Shah, R. W. Smalling, J. M. Rubin, and W. G. Scott, "Synergy and applications of combined ultrasound, elasticity, and photoacoustic imaging," in *Proc.-IEEE Ultrason. Symp.* pp. 405–415 (2006).
24. J. Shah, S. R. Aglyamov, K. Sokolov, T. E. Milner, and S. Y. Emelianov, "Ultrasound-based thermal and elasticity imaging to assist photothermal cancer therapy—preliminary study," in *Proc.-IEEE Ultrason. Symp.* pp. 1029–1032 (2006).
25. S. Sethuraman, S. R. Aglyamov, R. W. Smalling, and S. Y. Emelianov, "Remote temperature estimation in intravascular photoacoustic imaging," *Ultrasound Med. Biol.* **34**(2), 299–308 (2008).
26. J. Shah, S. Park, S. R. Aglyamov, T. Larson, L. Ma, K. Sokolov, K. Johnston, T. E. Milner, and S. Y. Emelianov, "Photoacoustic imaging and temperature measurement for photothermal cancer therapy," *J. Biomed. Opt.* **13**(3), 034024 (2008).
27. S. H. Wang, C. W. Wei, S. H. Jee, and P. C. Li, "Photoacoustic temperature measurements for monitoring of thermal therapy," *Proc. SPIE* **7177**, 71771S (2009).
28. G. Ku and L. H. V. Wang, "Deeply penetrating photoacoustic tomography in biological tissues enhanced with an optical contrast agent," *Opt. Lett.* **30**(5), 507–509 (2005).
29. IEEE standard for safety levels with respect to human exposure to radio frequency electromagnetic fields 3 kHz to 300 GHz, IEEE Std. C95.1, 1999 Ed.
30. Laser Institute of America, American National Standard for Safe Use of Lasers ANSI Z136.1-2000, American National Standard Institute, New York (2000).
31. *Handbook of Physical Quantities*, CRC Press, Boca Raton (1997).
32. J. A. D. Matthew, *CRC Handbook of Chemistry and Physics—Weast*, Vol. **33**, CRC Press, Boca Raton (1988).